Kinetic-contact-driven gigantic energy transfer in a two-dimensional Lennard-Jones fluid confined to a rotating pore

Paweł Karbowniczek and Agnieszka Chrzanowska
Institute of Physics, Cracow University of Technology, ul. Podchorążych 1, 30-084 Kraków, Poland
(Received 11 August 2017; revised manuscript received 7 October 2017; published 27 November 2017)

A two-dimensional Lennard-Jones system in a circular and rotating container has been studied by means of molecular dynamics technique. A nonequilibrium transition to the rotating stage has been detected in a delayed time since an instant switching of the frame rotation. This transition is attributed to the increase of the density at the wall because of the centrifugal force. At the same time the phase transition occurs, the inner system changes its configuration of the solid-state type into the liquid type. Impact of angular frequency and molecular roughness on the transport properties of the nonrotating and rotating systems is analyzed.

DOI: 10.1103/PhysRevE.96.053113

I. INTRODUCTION

In recent years one observes an increased interest in properties of confined fluids, liquids, and granular matter. Importance of such systems comes not only from the fact that they exhibit new features as compared to the bulk systems, but also because of their practical applications. First of all, the phase diagram of a fluid confined in a porous medium can be distinctively different from the one in the bulk due to the interaction with the walls of the pores and geometrical constraints. In the liquid phase, for instance, confinement induces layering of the particles at the wall and can completely change the freezing scenario, which becomes dependent mainly on the strength of the interaction between the wall and the inner system particles [1,2]. Interesting aspects of confinement include also, besides nonuniform density distribution [3–7], preferential adsorption in mixtures [8–12], surface phase transitions in thin liquid films [13,14], phase transitions in self-assembled monolayers [15,16], novel structures in liquid crystals [17] and lubrication films [18], and even possibility of glass transition [19]. Understanding the structure and transport properties of confined matter is also important for processes such as melting [20], wetting, adsorption, nucleation, and phase separation [21]. From the technological point of view, porous materials are important since they have many applications in chemistry and pharmaceutical industry [22,23].

The first theoretical description of fluids under confinement has been proposed by Henderson, Abraham, and Barker [24]. In this work the authors obtained and presented the density profile of a hard-sphere fluid in contact with a structureless wall by solving the Ornstein-Zernike equation. These investigations have been followed by Abraham and Singh perturbation theory [25], in which the structureless walls were treated as soft and cohesive (or repulsive). The problem of the wall interactions was a focus of a sequence of next works [26–30], whose aim was rather to find an effective form of the surface potential instead of considering the explicit intermolecular contributions. A detailed review of the research on the effects of confinement like layering or gas-liquid transition of different confined fluid systems by the use of both theoretical and simulation techniques has been given in the work of Gelb *et al.* [21].

Naturally, the interest in confined systems was quickly extended to nanofluidic transport properties like mass flow and heat transfer (see, for example, Refs. [31–34]). In addition to the confinement conditions, additional energy transfer can induce even more interesting effects. For example, recent studies [35] have proven that driven granular matter can have non-Maxwellian velocity distribution. Many aspects of molecular flow have been investigated theoretically mostly using nonequilibrium molecular dynamics, introduced by Hoover and Ashurst [36]. It has been shown that channel width, wettability, heat transfer, external forces, and geometry of confinement significantly influence the behavior of the above-mentioned flow and transport properties.

In studying properties of confined systems there are two distinct types of the approach. The first type concerns the case when the wall is smooth and structureless and the second type when the wall is rough. The inner system in confinement can be also treated as continuous medium (by the use of the Navier-Stokes description) or as a set of individual particles. Fully continuous models turn out, however, inefficient. Moreover, they fail at the level of few molecular diameters from the wall, where the influence of the wall becomes particularly strong [37,38]. Structureless models cannot describe then all the physical processes that might occur in microporous structures. When a flat wall is changed into even a slightly corrugated wall, then the dynamic behavior of a confined liquid can be drastically modified [39–41]. Being motivated by this conclusion, we already studied the influence of the wall particle size on the density profiles of the Lennard-Jones system confined in a structured circular geometry [42].

The current work extends our previous studies for the case of nonequilibrium and dynamical conditions. In particular, it presents a detailed description of a molecular system behavior in a two-dimensional rotating micropore. Section II presents the details of the atomistic model and computational aspects. Section III presents a nonequilibrium transition with a gigantic energy transfer from the rotating wall to the inner system that results in the global system rotation. A simple model describing this behavior has been proposed in Sec. IV. Energy transfer and influence of the system size on the transition to the rotating mode have been given in Sec. V. In Sec. VI we summarize our results.

II. MODEL AND COMPUTATIONAL DETAILS

We consider a two-dimensional circular container constructed from the Lennard-Jones particles with the linear

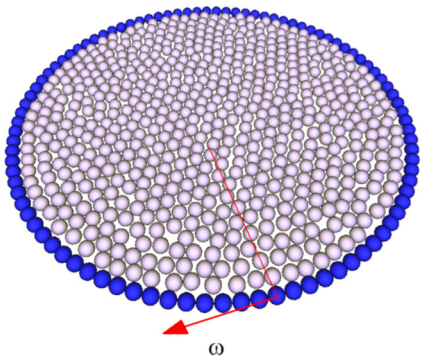

FIG. 1. Visualization of the studied system.

particle density equal to 1. The particles are placed inside. We assume that the edge particles are immobile in relation to each other, but they do interact with the internal system. The N confined particles interact via the Lennard-Jones potential [43], describing the interaction between a pair of neutral molecules:

$$U_{\text{inner}}(r) = 4\epsilon_{11}\left[\left(\frac{\sigma_{11}}{r}\right)^{12} - \left(\frac{\sigma_{11}}{r}\right)^{6}\right], \tag{1}$$

where ϵ_{11} and σ_{11} are the potential well depth and diameter of the inner system particles. In reality, walls and edges always influence molecular system in their vicinity, therefore we also assume an interaction describing such influence. In general, there are several known rules for choosing parameters of interaction; however, three of them are the most popular: the Lorentz-Berthelot [44,45], the Waldman-Hagler [46], and the Kong [47] one. In this paper, we use the Lennard-Jones potential, in which the interaction parameters fulfill the generally accepted Lorenz-Berthelot rules:

$$\sigma_{12} = \frac{\sigma_{11} + \sigma_{22}}{2} \tag{2}$$

and

$$\epsilon_{12} = \sqrt{\epsilon_{11}\epsilon_{22}}, \tag{3}$$

where ϵ_{22} and σ_{22} are the parameters of the potential describing the edge particles.

In Fig. 1 an example of typical configuration of the particle system is presented. The potential field originating from the assumed circular geometry at the point $z = (z_x, z_y)$ is calculated as

$$U_f(z,t) = \sum_{i=1}^{M} U_i(z - z_i(t)), \tag{4}$$

where M is the number of particles constructing the circular container and $z_i(t)$ are the positions of the edge particles at the time t. Since we focus on the influence of the container rotating with the angular frequency ω, the effective potential field will also depend on ω:

$$U_f(z,t) = \sum_{i=1}^{M} 4\epsilon_{12}\left[\left(\frac{\sigma_{12}}{\zeta_i(z,t)}\right)^{12} - \left(\frac{\sigma_{12}}{\zeta_i(z,t)}\right)^{6}\right], \tag{5}$$

with

$$\zeta_i(z,t) = \sqrt{\begin{array}{l}\left[z_x - Z\cos\left(\frac{2\pi i}{M} + \omega t\right)\right]^2 \\ +\left[z_y - Z\sin\left(\frac{2\pi i}{M} + \omega t\right)\right]^2\end{array}}, \tag{6}$$

where Z is the radius of the container. The origin of the Cartesian coordinates is chosen at the geometrical center of the molecular system. The wall particles have infinite mass and move only collectively as a rotating frame. This model takes into account only a single layer of the edge particles, yet it still serves as a realistic representation of the physical systems. In a general case, one can take into account more edge layers and consider corrections resulting from them.

The simulation performed is divided into two parts. In the first part an equilibrated initial configuration is prepared under assumption of periodic boundary conditions mimicking the bulk unlimited system. From such configuration a part conforming the size of the container is cut out and, then, placed inside the container. Simulation is further performed until the system reaches thermodynamic equilibrium. At the second stage of simulation the angular velocity of the container is abruptly turned on. The total energy of the inner system will be increasing now due to the interaction with the wall. Since the rotating container is assumed to maintain its angular frequency, the total energy will be not conserved and we will deal with the nonequilibrium NV system. All the simulations were performed using the velocity Verlet integration scheme [48,49] with the time step as small as $\Delta t = 0.0002$ to ensure the highest quality of the results in nonequilibrium conditions. The whole simulations were carried out for 5×10^5 time steps. Note that in our calculations we assumed the standard shifted-potential with a cutoff of 2.5σ, dimensionless reduced units, and equations simplified to relevant variables.

III. GIGANTIC ENERGY TRANSFER

As the first case we will consider the following conditions: the angular velocity of the nanopore is assumed as $\omega = 1$, its radius as $Z = 15\sigma_{11}$ (where σ_{11} is the inner system particle diameter), and the density of the inner system as $\rho = 0.95$. The particles of the inner system are of the same kind as the particles constituting the edge of the nanopore ($\sigma_{11} = \sigma_{22} = 1, \epsilon_{11} = \epsilon_{22} = 1$). At the beginning of the simulation the particles inside the nanopore are being initially equilibrated within the time equal to 10 to economize the whole space of the nanopore. Then, suddenly, the angular velocity of the container is turned on. Interaction with the edge particles will cause now an increase of the kinetic energy of the inner particles. Figure 2 presents all energy curves that characterize this process. During the simulation the kinetic energy increases very slowly until a certain value of time denoted as τ, above which one observes a sudden large jump. At this point the system enters a new dynamical stage in which all particles are moving in a collective manner. We will call it the rotating stage. Transition to this stage depends on the density of the system, the Lennard Jones interaction parameters, and the type of the edge particles. During the time τ from Fig. 2 the circular container underwent about three full rotations. Within this time the total potential energy of the system is negative which

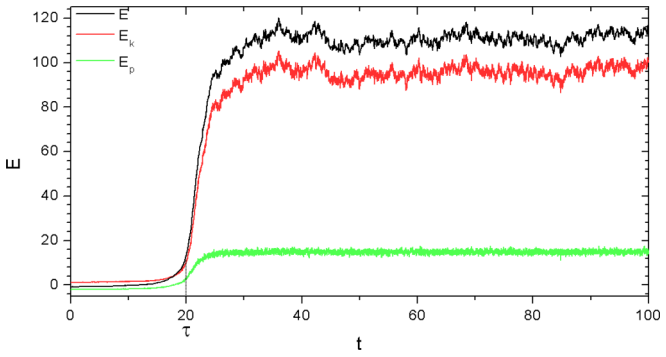

FIG. 2. Total energy E, kinetic energy E_k, and potential energy E_p time dependencies of the simulated particles in a container with the radius $Z = 15$ for $\sigma_{22}/\sigma_{11} = 1$, $\rho = 0.95$, and $\omega = 1$. Gigantic energy transfer occurs at the transition to the rotating stage. Note that the initial total energy is equal to -0.9.

denotes that on average the particles find themselves in the potential wells close to their minimums. In the rotating stage the potential energy is positive, which indicates that particles much departed from these positions.

From Fig. 2 it is also seen that the rotating stage comprises three characteristic regions. At the time of $t = \tau = 20$ one observes a very strong increase of all energies until about the time $t = 25$, then, in the next time region, increases are still strong until $t = 40$, when the energies attain almost constant levels. A the same time one observes strong fluctuations as well in the second as in the third part of the rotating stage. The total kinetic energy is about four times larger than the potential energy. The level of the potential energy seems to be preserved, whereas a small increase of the kinetic energy is noticeable, which is symptomatic for continuous heating of the system.

Figure 3 presents changes in the radial density profile. The initial crystal-like structure that manifests itself in well-defined

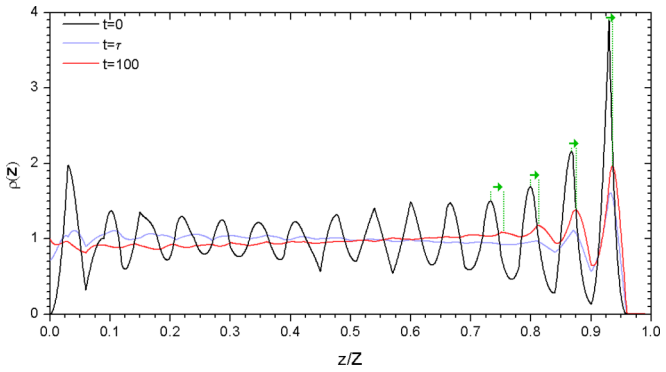

FIG. 3. Density as a function of distance from the center of the container of size $Z = 15$ obtained at the times: $t = 0$, $t = 20 = \tau$ (the beginning of the rapid increase of energy), $t = 100$ (the end of the simulation). Simulations were performed for $\sigma_{22}/\sigma_{11} = 1$, $\rho = 0.95$, and $\omega = 1$. The curves are smoothed over 10^4 time steps near a given point in time. The effect of centrifugal force is indicated by arrows showing small shift of the density peaks towards the edge of the geometry.

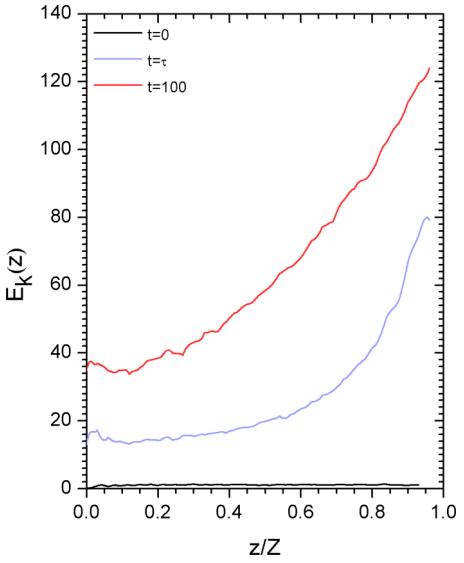

FIG. 4. Change of the profile of the kinetic energy as a function of distance from the center of the container obtained at different simulation times for $Z = 15$, $\sigma_{22}/\sigma_{11} = 1$, $\rho = 0.95$, and $\omega = 1$. The final kinetic energy profile is parabolic.

peaks (black solid line) is melting slowly. In the transition region there is no global structure in the density profile observed, there are only three fluid layers at the wall (blue solid line). After the transition to the rotating stage the density profile (red solid line) increases near the edge and decreases in the middle of the nanopore. Also the density peaks become lower and shift toward the edge of the geometry. The density peak shift near the wall is equal to about a dozen or so percent of the size of a particle after the transition, which is a big value when we take into account high packing of particles. These two effects are associated with the centrifugal force. It is an interesting observation that in the rotating stage one can still observe three visible layers of the fluid at the wall, whereas in the middle of the nanopore the density is uniform, indicating the liquid state.

Figure 4 shows changes of the profile of the kinetic energy as a function of distance from the center of the nanopore obtained at different simulation times. At the beginning the distribution is uniform (black solid line). At the transition to the rotating stage one observes a big increase of the kinetic energy at the wall that is propagating toward the center of the nanopore due to the transfer of the energy from the edge to the outer parts of the inner system. At the end of the simulation the kinetic energy profile calculated in a laboratory reference frame is parabolic. Note that since the kinetic energy profile is parabolic, the transverse velocity profile is linear. In this state, the particles rotate in accordance with the rotating container.

IV. MODELS OF THE ROTATING PLATES

To explain theoretically the behavior of the above kinetic energy two models will be considered, which form ideal reference models: hard rotating plate model and soft rotating plate model.

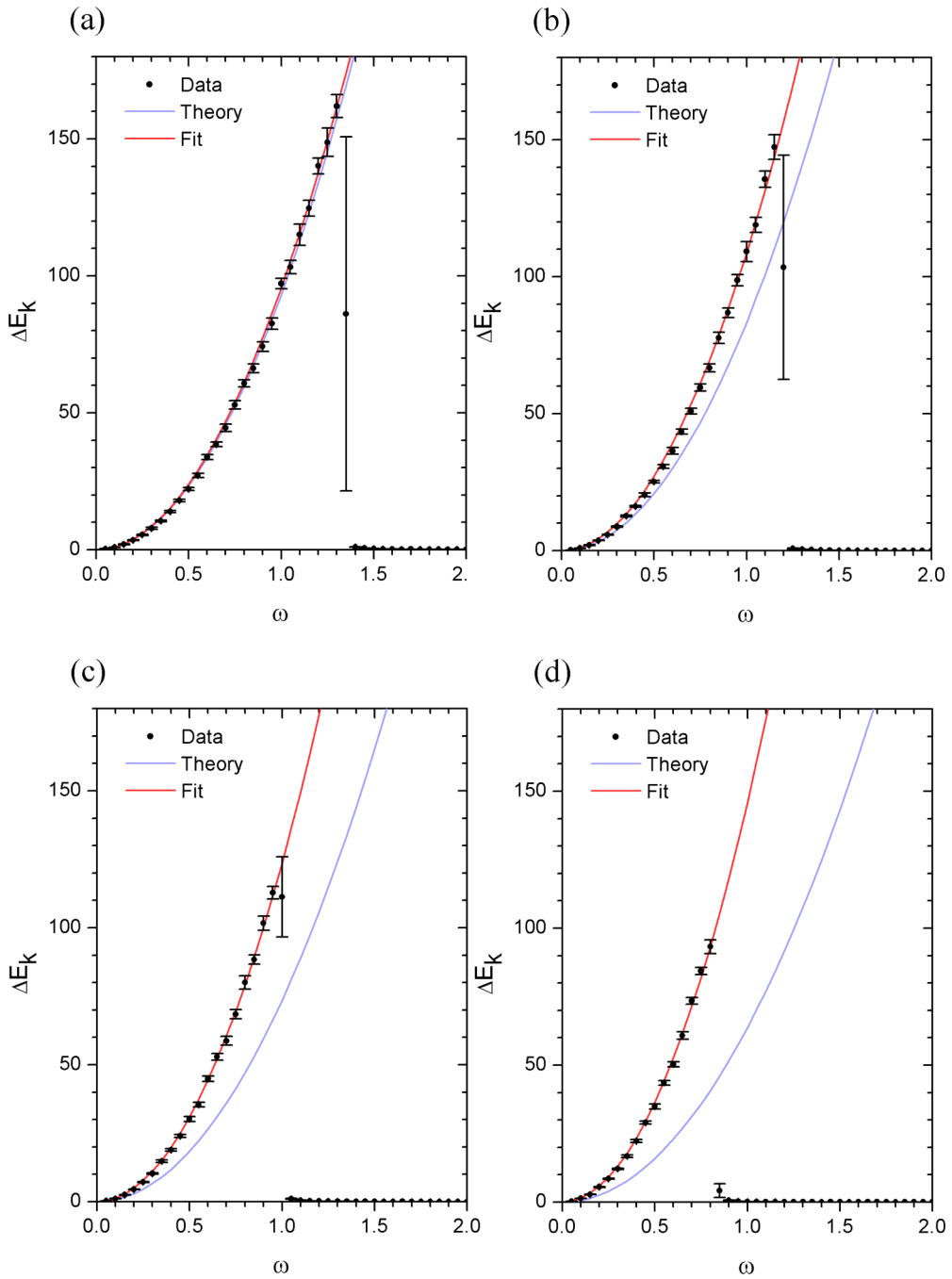

FIG. 5. Change of the kinetic energy for the roughness $\sigma_{22}/\sigma_{11} = 1$. The radius of the container is $Z = 15$. The angular frequency of the rotation ω varies from 0.05 to 2.00 with the step 0.05. Theoretical curve is due to the soft rotating plate model calculated using Eq. (10). Each panel shows the results for a different density: (a) $\rho = 0.95$, (b) $\rho = 0.85$, (c) $\rho = 0.75$, (d) $\rho = 0.65$.

A. Hard rotating plate

Let us consider a simplified rotating disk composed of N densely packed hard interacting particles (hard disks or hard spheres) of the diameter σ_{HD} and the mass $m = 1$. The last layer of the particles forms the edge of the container, where the radius of the container is Z. The moment of inertia of the inner system is

$$I \simeq \tfrac{1}{2} mN(Z - \sigma_{\mathrm{HD}})^2. \tag{7}$$

The average rotational kinetic energy of the inner system particle is then equal to

$$E_k = \frac{I\omega^2}{2N} = \frac{1}{4} m\omega^2 (Z - \sigma_{\mathrm{HD}})^2 = \frac{1}{4}\omega^2 (Z - \sigma_{\mathrm{HD}})^2. \tag{8}$$

Densely packed particles can only move around the main axis of rotation as their thermal motions are much smaller than the overall rotational movement. As a consequence, the kinetic energy increase is associated mainly with the rotational term.

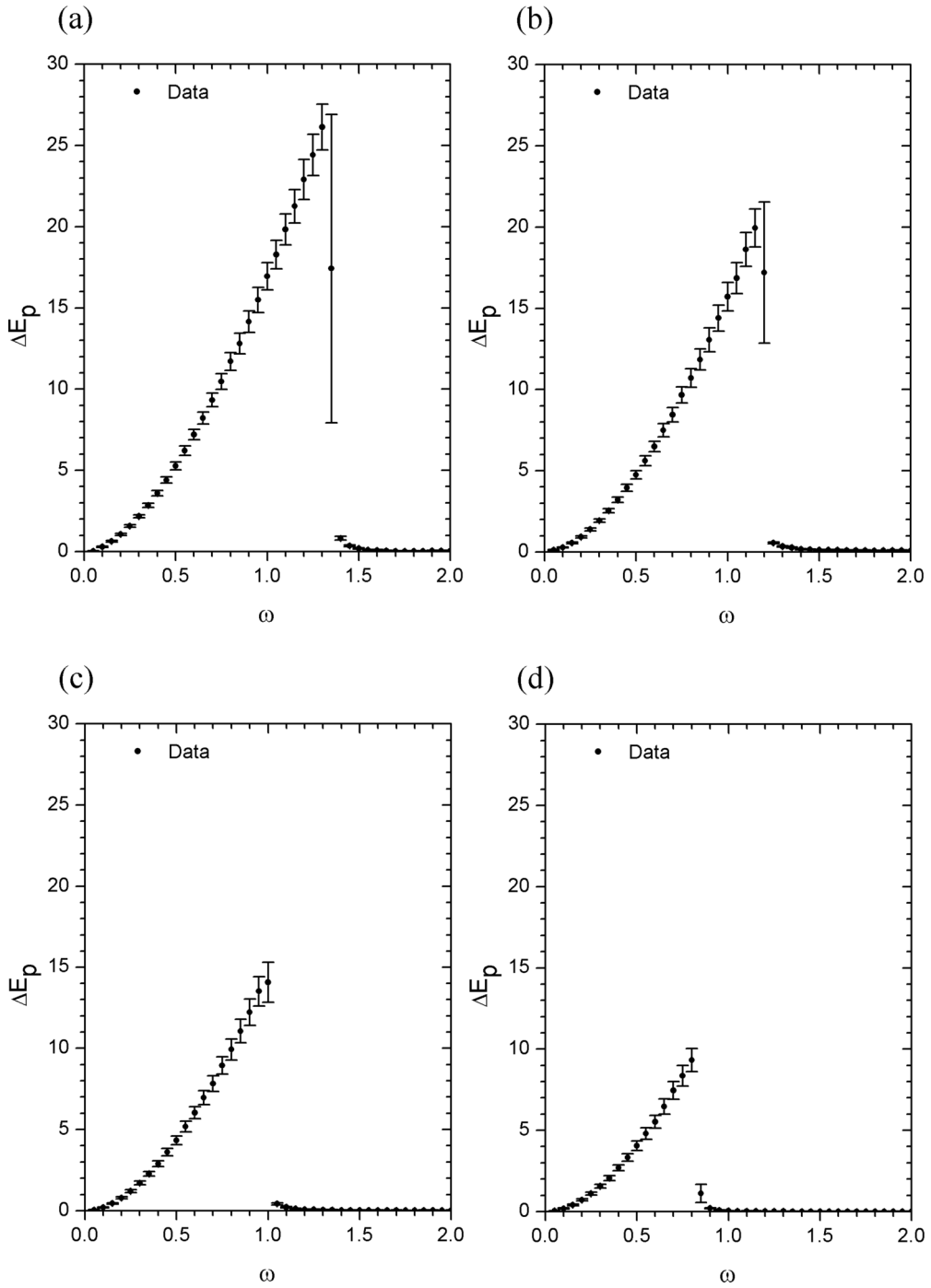

FIG. 6. Change of the potential energy for the roughness equal to $\sigma_{22}/\sigma_{11} = 1$. The radius of the container is $Z = 15$. The angular frequency of the rotation ω varies from 0.05 to 2.00 with the step 0.05. Each panel shows the results for a different density: (a) $\rho = 0.95$, (b) $\rho = 0.85$, (c) $\rho = 0.75$, (d) $\rho = 0.65$.

Let us call this model the hard rotating plate. This is an ideal situation, where the entire mass is rotating as a rigid body with no sliding of the particle layer over the another one.

B. Soft rotating plate

The soft rotating plate model refers to the system, when molecular motions become significant. For soft interacting particles, like in the Lennard-Jones case, we expect that the energy will increase twice:

$$E_k = \tfrac{1}{2}\omega^2(Z - \sigma_{12})^2, \tag{9}$$

because particles can move freely in the radial direction. Energy will be transferred from the wall to both rotational and radial degrees of freedom through thermalization process. In our work we have found out that the energy transfer is density, container size and edge particle size dependent. It might also be

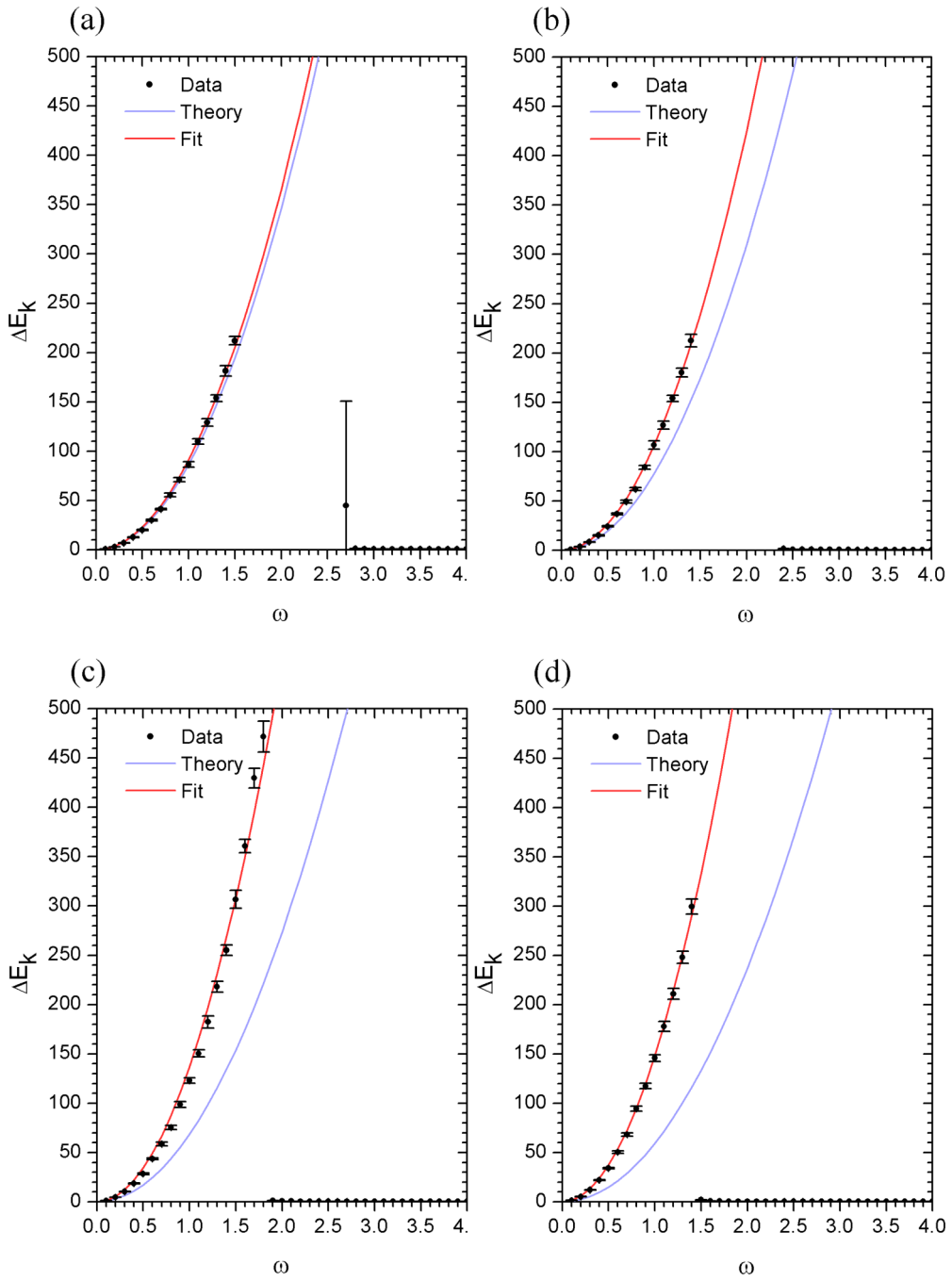

FIG. 7. Change of the kinetic energy for the roughness equal to $\sigma_{22}/\sigma_{11} = 2$. The radius of the container is $Z = 15$. The angular frequency of the rotation ω varies from 0.10 to 4.00 with the step 0.10. Theoretical curve is due to the soft rotating plate model. Each panel shows the results for a different density: (a) $\rho = 0.95$, (b) $\rho = 0.85$, (c) $\rho = 0.75$, (d) $\rho = 0.65$.

affected by nonuniformity in the density distribution due to the centrifugal force. Using this information we assumed a simple semiphenomenological equation, in which the amount of the kinetic energy transferred to the inner system is proportional to the dimensionless density:

$$E_k = \frac{1}{2}\frac{\rho}{\rho_0}\omega^2(Z-\sigma_{12})^2 = \frac{1}{2}\rho\omega^2(Z-\sigma_{12})^2, \qquad (10)$$

which properly reproduced the data from simulations at least for small particles forming the edge of the geometry over the studied density range.

Note that while using a concept of temperature a need arises to consider the effective radius of the geometry $Z - \sigma_{12}$. This can be done using the Barker-Henderson theory for the effective hard disk diameter [50,51], which depends on the temperature of a molecular system. As a result the expected kinetic energy per particle in the soft rotating plate model would

be proportional to $(Z - \int_0^{\sigma_{12}} \{1 - \exp[-\beta U_{\text{inter}}(r)]\} dr)^2$. In our case, however, change of the effective diameter of the edge particle is negligible, when compared to the whole system size (see Fig. 3).

V. KINETIC CONTACT BREAKUP

Here, we analyze gigantic energy transfer and kinetic contact breakup. By the contact condition we understand a situation in which particles find themselves in or close to the their most preferred positions within the potential wells. This manifests itself in the negative value of the potential energy. If such a contact is broken (kinetic contact breakup) according to the kinetic conditions, the potential energy becomes positive, which means that the positions of the particles moved toward the steep and repulsive walls of the potential. Such understood a contact should be distinguished from the no-slip condition for a part of the system at the wall. It is possible that what really takes place is that one observes the no-slip condition at the wall but the particles are out of their equilibrium preferred positions. The strong increase of the potential energy and the kinetic contact breakup we observed are associated with the transition to the rotating stage. These properties will depend on several conditions. First of all, they are influenced by the angular velocity of the container. Besides this influence, the properties of the nanopore wall play a decisive role here: the size of the constituent particles and the potential parameters of the interaction between the inner system and the wall particles.

A. Kinetic and potential energies

First, we study the impact of the edge particle size on the inner system properties. For this purpose, simulations were carried out for the container of the radius equal to 15. The most important parameter here is the ratio of the edge particle size to the inner particle size σ_{22}/σ_{11}, which will be referred to as roughness. We used such an idea, because roughness at the atomistic scale is often modeled by varying the size and spacing between solid atoms [52–54]. Note that roughness modeled in that way is proportional to the wall potential field curvature [55]. When the roughness σ_{22}/σ_{11} attains the unity value, then the particles of the inner system have the same size as the edge particles. We kept the inner particle size as $\sigma_{11} = 1$ and varied the size of the nanopore particles so that the parameters of roughness were equal to $1/2$, 1, and 2. It should be noted here that the smaller the edge nanopore particles are, the smaller the area is, when the potential field is significant and, also, the effective potential field becomes more uniform. Simulations were also carried out for different densities of the inner system: $\rho = 0.65$, 0.75, 0.85, and 0.95.

In Figs. 5–8, changes of the kinetic and potential energy observed with respect to the angular frequency are shown for different roughnesses. These energies are averages calculated from the values of the data at the last parts of the rotating stage (see Fig. 2). In all cases, the gain of the energy is very strong.

In Fig. 5, one notices that for larger densities the simple theoretical formulas emerging from the soft rotating plate model seems to hold the best. The deviation from the soft rotating plate increases while decreasing density. Another characteristic feature is that upon decreasing density of the system, the angular velocity, at which the rotating stage is obtained, gradually diminishes. This can be attributed to the fact that less dense systems have smaller inertia and smaller potential energy due to larger distances among particles. Figure 6 presents the behavior of the potential energies for the same cases as in Fig. 5. Analyzing Figs. 5–8, one can also deduce that the particles gain larger amounts of energy for larger roughnesses, i.e., in the case when the effective potential field is nonuniform and acts at larger areas.

The presented error bars are determined by big fluctuations present at the rotating stage. When the angular velocity considered is so large that our time of the simulations happens to be within the transition point then error bars can be very big like in Figs. 5(a) and 5(b). If the angular velocity is even larger then we are not entering the rotating stage within our maximal simulation time; hence, in the above figures energy increases are at zero level. This fact, however, only means that the simulation times should be much longer if we would like to encounter the rotating stage.

Figure 7 presents energies for the case when edge particles are twice the size of the particles inside the nanopore. Here the gain of energy is larger than in the previous case within the same time of the simulations. This is attributed to the fact that the well of the potential covers a much larger area so the effective interaction at the nanopore wall is stronger. Here again one observes for dense system that the soft plate applies. For less dense systems there are strong differences, which indicate that such systems are much warmer.

For roughness equal to $1/2$ the edge is smoother, but in this case, shown in Fig. 8, the transfer of the energy from the edge into the system is a much weaker process. It is an interesting thing here that Eq. (10) fits the data well for all densities used. Another observation is that for this roughness it takes much longer simulation time to achieve the rotating stage in this case.

B. Time of the transition and surplus kinetic energy

In Fig. 9 we present times of rapid transition for the system of the size $Z = 15$, the roughness 1, and the density 0.95. The main outcome here is observation that the time required for this transition grows exponentially with angular frequency. In practice it means that much larger times are needed in simulation to observe the discovered effect.

The initial data points for the kinetic energy changes presented in Figs. 5, 7, and 8 can be well fitted to a parabolic curve:

$$\Delta E_k = A\omega^2, \tag{11}$$

where A is a proportionality constant. In general, this kinetic energy change ΔE_k consists of the rotational part and the surplus part. In Eq. (9) they are equal to $\omega^2(Z - \sigma_{12})^2/4$ and $\alpha\omega^2(Z - \sigma_{12})^2/4$. When $\alpha = 0$ then we have the ideal hard rotating plate and when $\alpha = 1$ then we have the ideal soft rotating plate. Using Eq. (10) the kinetic energy can be decomposed similarly into $\rho\omega^2(Z - \sigma_{12})^2/4$ and $a\rho\omega^2(Z -$

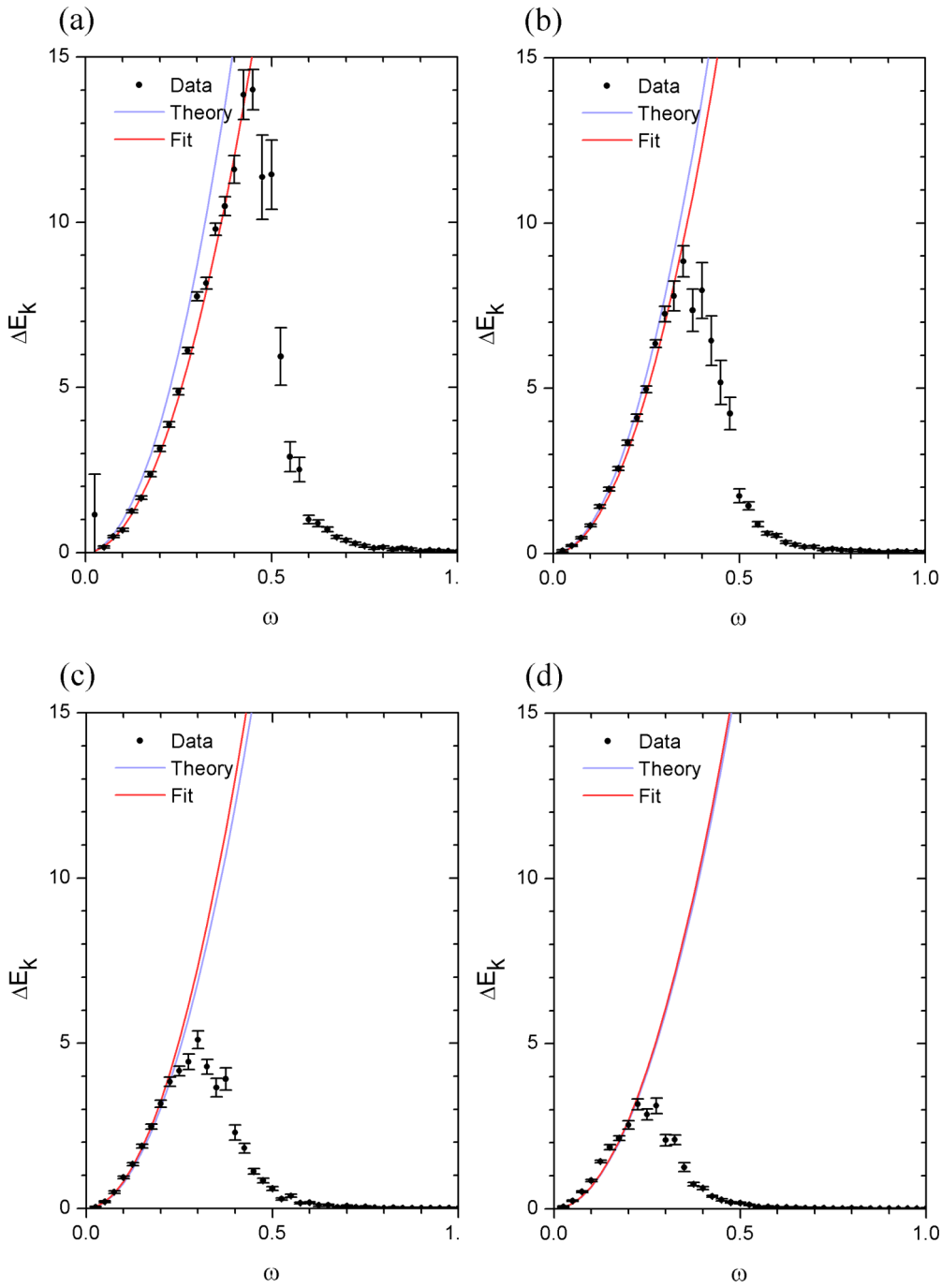

FIG. 8. Change of the kinetic energy for the roughness equal to $\sigma_{22}/\sigma_{11} = 1/2$. The radius of the container is $Z = 15$. The angular frequency of the rotation ω varies from 0.025 to 1.000 with the step 0.025. Theoretical curve is due to the soft rotating plate model. Each panel shows the results for a different density: (a) $\rho = 0.95$, (b) $\rho = 0.85$, (c) $\rho = 0.75$, (d) $\rho = 0.65$.

$\sigma_{12})^2/4$, where

$$a = \frac{4A}{\rho(Z - \sigma_{12})^2} - 1. \tag{12}$$

We present the results of a parameters since Eq. (10) holds better for all densities used for one type of the edge particles. All the results can be, however, scaled using different equations used to fit the data. Here, for example, $\alpha = \rho(1 + a) - 1$. Therefore, Eq. (12) gives information about the type of the additional kinetic energy transfer. Figure 10 shows a coefficient calculated on the basis of Figs. 5, 7, and 8. Additional blue and red lines represent the ideal hard and soft plate models. For the roughnesses 1 and 2 and higher densities, one can see almost the ideal soft rotating plate character. The surplus kinetic energy increases with decreasing density and it is bigger than the ideal soft plate model. Within the simulation time the energy gain for roughness equal to 1/2 is very slow and, therefore, the a parameter differs significantly from the cases with bigger roughnesses. For longer simulations, we

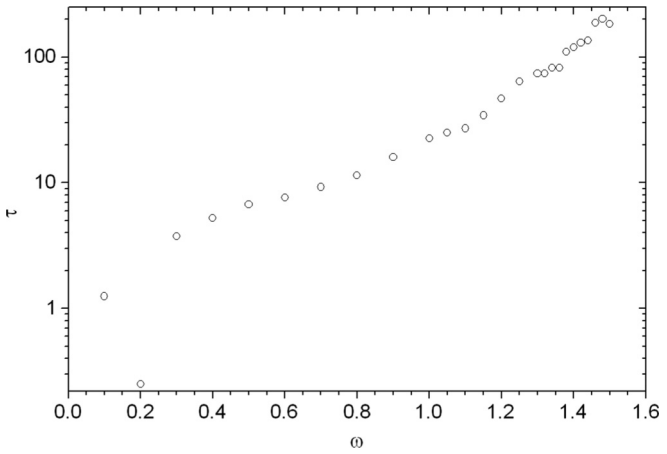

FIG. 9. Times of the rapid transition for the system of the size $Z = 15$, the roughness $\sigma_{22}/\sigma_{11} = 1$ and the density $\rho = 0.95$.

expect that the surplus kinetic energy for a case with roughness of $1/2$ will be approaching slowly the value characteristic for the ideal soft plate.

C. Influence of the system size on the transition time to the rotating stage

Detailed simulations have been also performed to investigate the a parameter change for different sizes of the container (see Fig. 11). In these studies the roughness was equal to 1 and the density was equal to 0.95. The simulations revealed that the larger the system is, the more time is needed for the transition to the rotating stage. This effect comes from the fact that for greater values of the angular frequency the outside particles need more time to transfer energy to the system, while the transmission rate is hindered by the geometry. Figure 12, based on results from Fig. 11, shows a decrease of the a parameter with enlarging the system and the container. Observed values agree with the expectations for the macroscopic systems, where the surplus kinetic energy is expected to be equal to

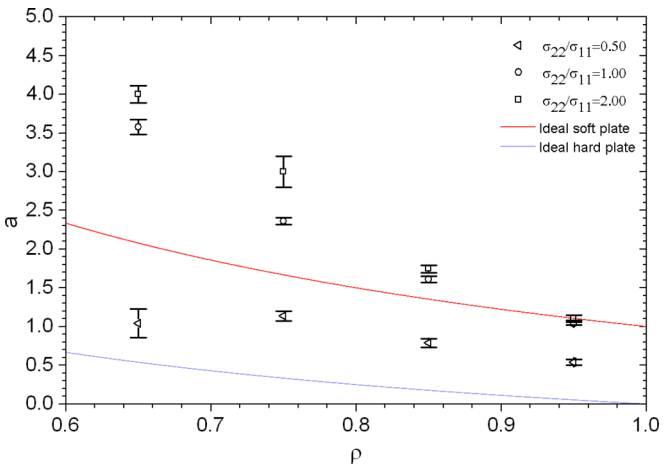

FIG. 10. a parameter obtained for the time $t = 100$. The lines indicating the ideal hard and soft plates are presented in blue and red colors.

0, which means that the whole system starts to rotate without destruction of a crystalline structure.

VI. SUMMARY

The dynamical transition of the solid system of Lennard-Joners two-dimensional particles confined to a rotating circular nanopore to the rotating stage accompanied by a gigantic energy transfer from the nanopore walls to the inner system and the breakup of the particles contact was observed. The transition process has two stages. In the first stage one observes melting of the solid structure that is accompanied by a slow energy gain. The second stage is the fast transition to the rotating state, at which the above-mentioned large increase of the inner system energy occurs. The molecular mechanism is as follows. Initially, upon switching circulation of the nanopore, only the first fluid layer close to the wall is pulled by the edge particles resulting in the energy increase proportional to $\omega^2(Z - \sigma_{12})^2$, similarly as for the edge particles. The first layer interacts with the next one, thus one observes energy transmission toward the center of the system. At this stage, strong layering at the wall was observed together with the destruction of the positional order in the center of the system. At a certain time a very fast energy transfer occurs. The potential energy of the particles becomes positive, which means that the particles are no longer situated within local potential wells. Because of the gigantic kinetic energy transfer the whole system starts to rotate. The final effect (movement of the internal system in accordance with the wall) is similar to the experiments in a planar geometry, in which the shear rate (counterpart of our angular frequency) disrupts the change of the density peaks and flow behavior of the inner system (see, for example, Ref. [56]). However, due to the adopted geometry, the impact of centrifugal force seems to play a decisive role in driving the system into the rotating stage. Increase of the density peaks and the shift of their position close to the walls as the effect of the centrifugal force is, of course, determined by the curvature of the particles trajectory. As a result, a fraction of the particles have been pushed toward steep walls of the potential wells and the interaction of the inner particles and the wall particles is enhanced, as is the transfer of the energy to the inner system. This effect will not be present if the particles are considered in the slit geometry. In the papers published so far on the confined systems in a slit geometry, no gigantic energy transfer has been observed [15,18,41,56]. These works, however, consider flows of fluids or liquids, no solids under shear.

We studied the transition to the rotating stage with respect to different molecular and geometrical factors. One of the most important factors is the parameter of roughness that was defined as the ratio of the edge particle size to the inner system particle size. We confirmed importance of roughness in a surface driving transitions in molecular systems. The value of roughness influences the potential energy field close to the nanopore edge, hence the geometry and the size of the wall particles matters. For the smaller edge particles there is observed a lower energy transfer in the same time unit as in the case of larger edge particles. The influence of the system size, its density, and angular frequency on the kinetic and potential energy of the system have been also studied for

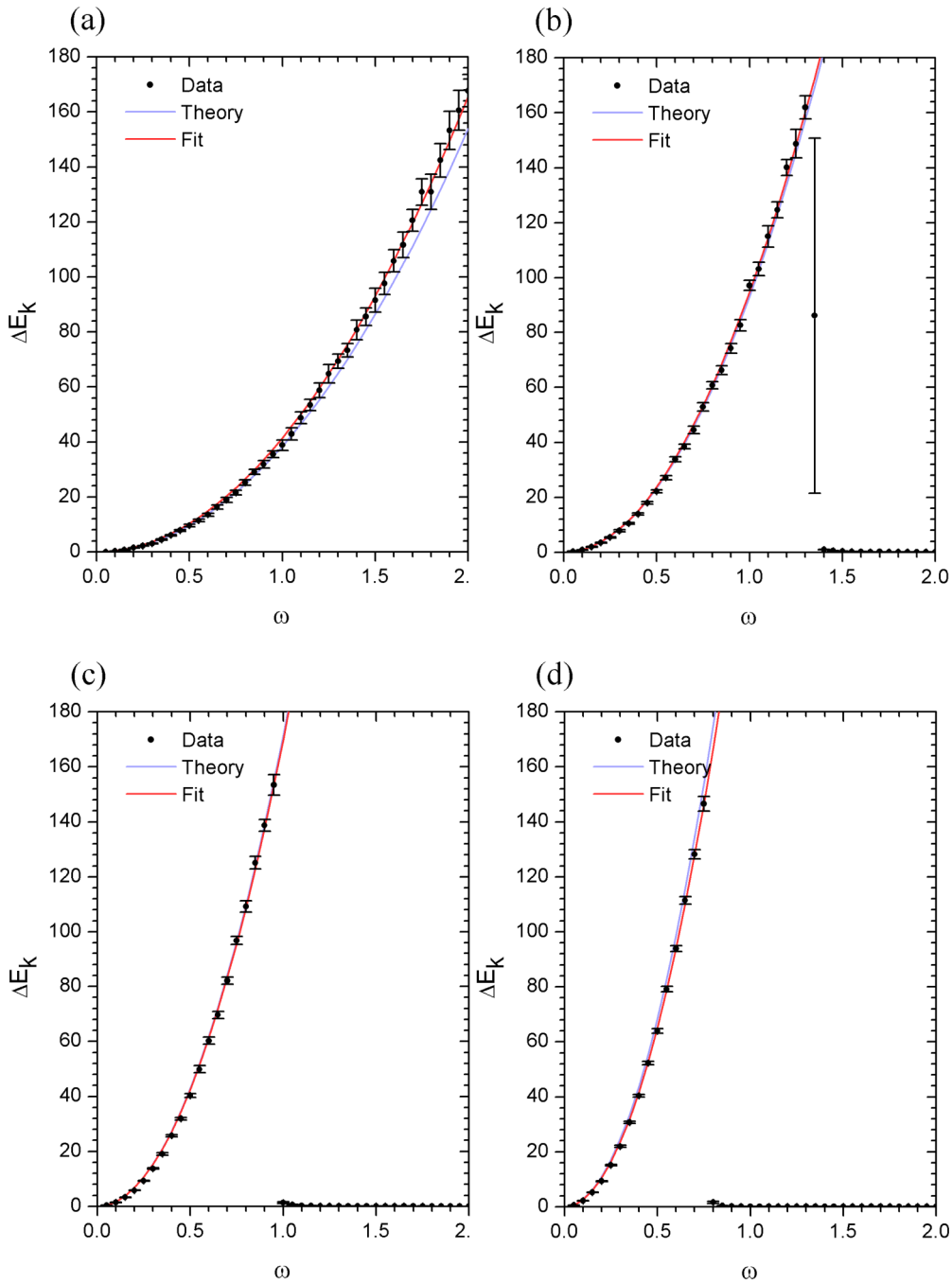

FIG. 11. Change of the kinetic energy for the roughness σ_{22}/σ_{11} equal to 1 and the density $\rho = 0.95$. The radius of the container Z varies from 10 (panel (a)) to 25 (panel (d)) with the step 5. The angular frequency of the rotation ω varies from 0.05 to 2.00 with the step 0.05.

several sets of exemplary values. At the first place one can point here at the dependence of the observed effect on the size of the system, which suggests that this transition can be a nanoscopic effect. If it is so, such a breaking of the solid structure by the motion of the container walls and putting the system in the rotating stage would be not only a very interesting and intriguing phenomenon but also of great importance for nanotechnological applications.

In our simulations, initially equilibrated NVE system was placed inside the container and then it was driven out of equilibrium by the energy transfer from the rotating walls. The potential and the kinetic energy transfers were not restricted. The simulations were performed without considering any outflux of the thermal energy and, also, without even using the concept of the temperature; hence, the presented results show the pure effect of the influence of the rotating wall on the inner system in terms of the kinetic and potential energies. The concept of the temperature in small systems is not well defined—it is not possible to take the thermodynamic limit, which is required by the statistical definition of the temperature. The temperature concept becomes even more problematic if the system is in a nonequilibrium state (see

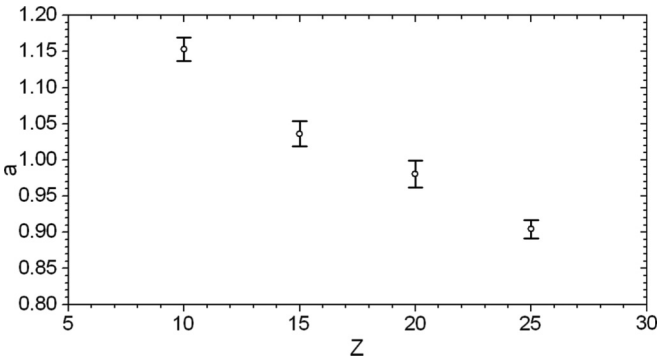

FIG. 12. Surplus kinetic energy parameter a changes with different container radius.

the discussion in the overview paper about the temperature concept in nonequilibrium states [57]). There is, of course, the possibility to propose a new definition of the small systems temperature, similarly as the attempts have been made to propose granular temperature in granular media [57], yet this problem we leave for future considerations. We also realize that in more realistic systems an outflux of the thermal energy to a greater or a lesser degree is always present. This would be an interesting task to extend the above results for the cases with an energy outflux. Considering such an effect requires an adoption of numerical thermostat. In principle, there are many ways to apply thermostats in confined matter [58,59] and, in fact, each reasonable method should be checked and analyzed in detail. Nevertheless, the results presented so far for the pure effect of an influence of the wall movement on the confined system can be a good springboard for further analysis.

Our predictions require confirmation from the experimental works. Whereas the nano-scale experiments with the rotating container can be hard to perform, one can see a real chance to observe them in colloidal systems, which are more controllable. Although most of the colloids tend to interact via the hard core rather than the Lennard Jones potential rules, one can still find some works where the Lennard-Jones [60] or Yukawa [61] potentials are being applied. Experiments, like the one presented in the paper, can be easily performed in two-dimensional colloidal science whether in a planar geometry or for a thin film confined between two walls.

[1] C. Alba-Simionesco, B. Coasne, G. Dosseh, G. Dudziak, K. E. Gubbins, R. Radhakrishnan, and M. Sliwinska-Bartkowiak, J. Phys.: Condens. Matter **18**, R15 (2006).
[2] M. Miyahara and K. E. Gubbins, J. Chem. Phys. **106**, 2865 (1997).
[3] J. J. Magda, M. Tirrel, and H. T. Davis, J. Chem. Phys. **83**, 1888 (1985).
[4] B. K. Peterson, K. E. Gubbins, G. S. Heffelfinger, U. Marini Bettolo Marconi, and F. van Swol, J. Chem. Phys. **88**, 6487 (1988).
[5] A. Yethiraj and C. K. Hall, J. Chem. Phys. **95**, 1999 (1991).
[6] K. G. Honnell and C. K. Hall, J. Chem. Phys. **95**, 4481 (1991).
[7] Y. Komatsu and H. Tanaka, Phys. Rev. X **5**, 031025 (2015).
[8] S. Sokolowski and J. Ficher, Mol. Phys. **71**, 393 (1990).
[9] L. Perez, S. Sokolowski, and O. Pizio, J. Chem. Phys. **109**, 1147 (1998).
[10] A. Yethiraj and C. K. Hall, Mol. Phys. **73**, 503 (1991).
[11] G. Rother, D. Woywod, M. Schoen, and G. H. Findenegg, J. Chem. Phys. **120**, 11864 (2004).
[12] A. Phan, D. R. Cole, and A. Striolo, Langmuir **30**, 8066 (2014).
[13] J. Klein and E. Kumacheva, Physica A (Amsterdam) **249**, 206 (1998).
[14] S. T. Cui, P. T. Cummings, and H. D. Cochran, J. Chem. Phys. **114**, 7189 (2001).
[15] L. Ramin and A. Jabbarzadeh, Langmuir **29**, 13367 (2013).
[16] C. D. Lorenz, J. M. D. Lane, M. Chandross, M. J. Stevens, and G. S. Grest, Langmuir **25**, 4535 (2009).
[17] D. de las Heras and E. Velasco, Soft Matter **10**, 1758 (2014).
[18] A. Jabbarzadeh, P. Harrowell, and R. I. Tanner, J. Phys. Chem. B **111**, 11354 (2007).
[19] B. Zhang and X. Cheng, Phys. Rev. Lett. **116**, 098302 (2016).
[20] X. Sun, Y. Li, Y. Ma, and Z. Zhang, Sci. Rep. **6**, 24056 (2016).
[21] L. D. Gelb, K. E. Gubbins, R. Radhakrishnan, and M. Sliwinska-Bartkowiak, Rep. Prog. Phys. **62**, 1573 (1999).
[22] R. F. Cracknell, K. E. Gubbins, M. Maddox, and D. Nicholson, Account Chem. Rev. **28**, 281 (1995).
[23] K. E. Gubbins, Chem. Eng. Prog. **86**, 42 (1990).
[24] D. Henderson. F. F. Abraham, and J. A. Barker, Mol. Phys. **31**, 1291 (1976).
[25] F. F. Abraham and Y. Singh, J. Chem. Phys. **67**, 2384 (1977).
[26] W. A. Steele, Surf. Sci. **36**, 317 (1973).
[27] C. Lastoskie, K. E. Gubbins, and N. Quirke, J. Phys. Chem. **97**, 4786 (1993).
[28] P. Olivier, W. B. Conklin, and M. von Szombathely, Stud. Surf. Sci. Catal. **87**, 81 (1994).
[29] W. A. Steele, J. Phys. Chem. **82**, 817 (1978).
[30] W. A. Steele, Chem. Rev. **93**, 2355 (1993).
[31] I. Benjamin, Annu. Rev. Phys. Chem. **48**, 407 (1997).
[32] H. Chen, Z. Zheng, Z. Chen, and X. T. Bi, Entropy **18**, 2 (2016).
[33] H. N. Yoshikawa, A. Meyer, O. Crumeyrolle, and I. Mutabazi, Phys. Rev. E **91**, 033003 (2015).
[34] A. V. Zakharova and A. A. Vakulenko, J. Chem. Phys. **143**, 104902 (2015).
[35] C. Scholz and T. Poschel, Phys. Rev. Lett. **118**, 198003 (2017).
[36] W. G. Hoover and W. T. Ashurst, Adv. Theor. Chem. **1**, 1 (1975).
[37] J. S. Hansen and J. T. Ottesen, Microfluid. Nanofluidics **2**, 301 (2006).
[38] F. Sofos, T. E. Karakasidis, and A. Liakopoulos, Contemp. Eng. Sci. **2**, 283 (2009).
[39] L. Bocquet and J. L. Barrat, Phys. Rev. E **49**, 3079 (1994).
[40] L. Guo, S. Chen, and M. O. Robbins, Phys. Rev. Fluids **1**, 074102 (2016).
[41] N. V. Priezjev, Phys. Rev. E **80**, 031608 (2009).
[42] P. Karbowniczek and A. Chrzanowska, Acta Phys. Pol. B **44**, 1209 (2013).
[43] J. E. Lennard-Jones, Proc. R. Soc. London A **106**, 463 (1924).
[44] H. A. Lorentz, Ann. Phys. (Berlin) **12**, 127 (1881).
[45] D. Berthelot, C. R. Acad. Sci. **126**, 1703 (1889).

[46] M. Waldman and A. T. Hagler, J. Comput. Chem. **14**, 1077 (1993).
[47] C. L. Kong, J. Chem. Phys. **59**, 2464 (1973).
[48] W. C. Swope, H. C. Andersen, P. H. Berens, and K. R. Wilson, J. Chem. Phys. **76**, 637 (1982).
[49] M. Tuckerman, B. J. Berne, and G. J. Martyna, J. Chem. Phys. **97**, 1990 (1992).
[50] J. A. Barker and D. Henderson, J. Chem. Phys. **47**, 4714 (1967).
[51] D. Henderson and J. A. Barker, Phys. Rev. A **1**, 1266 (1970).
[52] J. Gao, W. D. Luedtke, and U. Landman, Tribol. Lett. **9**, 3 (2000).
[53] A. Jabbarzadeh, J. D. Atkinson, and R. I. Tanner, Phys. Rev. E **61**, 690 (2000).
[54] T. M. Galea and P. Attard, Langmuir **20**, 3477 (2004).
[55] L. Guo, S. Chen, and M. O. Robbins, Phys. Rev. E **93**, 013105 (2016).
[56] A. Jabbarzadeh, J. D. Atkinson, and R. I. Tanner, J. Chem. Phys. **110**, 2612 (1999).
[57] J. Casas-Vazquez and D. Jou, Rep. Prog. Phys. **66**, 1937 (2003).
[58] X. Yong and L. T. Zhang, J. Chem. Phys. **138**, 084503 (2013).
[59] S. De Luca, B. D. Todd, J. S. Hansen, and P. J. Daivis, J. Chem. Phys. **140**, 054502 (2014).
[60] L. Angelani, G. Foffi, F. Sciortino, and P. Tartaglia, J. Phys.: Condens. Matter **17**, L113 (2005).
[61] M. Brunner, C. Bechinger, W. Strepp, V. Lobaskin, and H. H. von Grunberg, Europhys. Lett. **58**, 926 (2002)